Articles

α-DNA, a Single-Stranded Secondary Structure Stabilized by Ionic and Hydrogen Bonds: $d(A^+\text{-}G)_n$[†,‡]

Mary Claire Shiber, Laurence Lavelle, John A. Fossella, and Jacques R. Fresco*

Department of Molecular Biology, Princeton University, Princeton, New Jersey 08544-1014

Received December 19, 1994; Revised Manuscript Received July 3, 1995[⊗]

ABSTRACT: A novel nucleic acid secondary structure, exemplified by $d(A^+\text{-}G)_{10}$, is formed by an intramolecular, cooperative, acid-induced, coil → helix transition. The helix is apparently left-handed, lacks base stacking and pairing, and is maintained by hydrogen and ionic bonds between dA^+ "side-chain" residues (with electropositive hydrogens $-N_6H_2$, $-N_1{}^+H$) and the phosphodiester backbone. Modeling indicates that those dA^+ residues lie approximately parallel to the helix axis, interacting with the $n-1$ backbone phosphates (with electronegative oxygens), somewhat like the −C=O···H−N− longitudinal interactions in a protein α-helix. Moreover, the intervening dG side-chain residues are extrahelical, as are amino acid side chains of an α-helix.

All currently recognized types of nucleic acid secondary structure involve helical stacks of bases. Such stacks occur in single strands, in base pairs of hairpins formed by single strands, in base pairs of two-stranded complexes, in base triplets of three-stranded structures, and in base quartets of four-stranded complexes.

In this paper, we provide details of an entirely different type of nucleic acid helical *secondary structure*, one that does not depend for its stabilization on helically wound stacks of bases or base pairs. Rather, this novel type of secondary structure encompasses single strands of the repeating homopurine doublet sequence $d(A\text{-}G)_n$ helically twisted by an unusual combination of ionic and hydrogen (H) bonds essentially parallel to the helix axis.

We first came upon this nucleic acid secondary structure in the course of investigating the molecular properties of $d(A\text{-}G)_{10}$, which displays an intense differential absorption of circularly polarized light (CD) without concomitant development of hypochromism in the near-ultraviolet (UV) when the pH is reduced from neutrality. Additional observations enabled attribution of this unusual dichotomy in optical properties to a single-stranded helical secondary structure stabilized largely by Coulombic interactions between negatively charged backbone phosphates and distal protonated dA (dA^+) residues that do not overlap with their nearest neighbor dG residues. Although these properties made it possible to deduce some regular features of the secondary structure of $d(A^+\text{-}G)_{10}$, direct evidence for many structural details was lacking (Dolinnaya & Fresco, 1992; Dolinnaya et al., 1993). We therefore undertook spectroscopic and molecular modeling studies, which confirm and solidify the inferred secondary structure. Nuclease sensitivity was also evaluated for comparison with that of other types of nucleic acid conformations.

EXPERIMENTAL PROCEDURES

S1 Nuclease Digestion. $d(A\text{-}G)_{10}$ was synthesized and purified to homogeneity (Dolinnaya & Fresco, 1992); dT_{21} (Midland Certified Reagent Co.) was shown to be greater than 95% pure (Fossella et al., 1993). Concentrations are in terms of residues. 5′-^{32}P-end-labeled $d(A\text{-}G)_{10}$ and $d(T)_{21}$ were purified by 16% denaturing PAGE, eluted into 10 mM Tris-HCl/0.1 mM EDTA, pH 7.4, and desalted with Sephadex G-25 (Pharmacia) in H_2O. Reaction mixtures contained 0.01 M NaOAc, pH 4.0/2.02 × 10^{-1} mM $d(A\text{-}G)_{10}$ or $d(T)_{21}$/6 × 10^{-3} mM corresponding labeled oligomer/1 mM $ZnCl_2$, and 5 units S1 nuclease (U.S. Biochemicals). After incubation at 22 °C for 5 min, then at 5, 20, or 40 °C for 10 min, digestion was initiated with S1 nuclease and $ZnCl_2$. Digestions were halted by removing 5 μL aliquots at 0.5, 1, 2, 5, 10, 15, 30, and 60 min to 4 μL of loading dye (70% formamide/0.1% xylene cyanol/0.1% bromophenol blue/57 mM EDTA, pH 7.5) and freezing. Frozen samples were heated at 90 °C for 5 min prior to loading on a 22% denaturing gel. PAGE was at 50 V/cm until the bromophenol blue migrated 20 cm. The percent full-length oligomer remaining at each time point was determined after autoradiography of wet gels and scintillation counting of cut bands of full-length oligomer and digestion products.

UV Perturbation Spectroscopy. Spectra were recorded (Dolinnaya & Fresco, 1992) at indicated temperatures, corrected for solvent absorbance and expansion, and difference spectra were calculated by computer. Each *P* spectrum was the difference between spectra in 0.01 M NaOAc, at either pH 3.0 or pH 4.0, both with and without 50% (w/v)

[†] This work was supported by a grant from the National Institutes of Health to J.R.F. (GM42936). L.L. was supported by a predoctoral training grant from the National Institutes of Health (GM08309) and aided by an Autodesk educational software grant.

[‡] This is paper no. 22 in the series entitled *Polynucleotides*, of which the last is Lavelle and Fresco (1995). On the occasion of his 75th birthday, this paper is dedicated to Paul Doty, with whom the first paper in this series was written (Fresco & Doty, 1957).

* To whom correspondence should be addressed.

[⊗] Abstract published in *Advance ACS Abstracts,* September 1, 1995.

0006-2960/95/0434-14293$09.00/0

ultrapure sucrose (Boehringer). The 60−5 °C *P difference* spectrum was calculated as the difference between the *P* spectra at those two temperatures.

^{31}P NMR Spectroscopy. Spectra were recorded on a Bruker WM250 spectrometer at 101.2 MHz of $d(A^+\text{-}G)_{10}$ at 20, 30, and 40 °C (10016, 5000, and 4600 scans were computer averaged, respectively). The signal to noise was enhanced by application of a line broadening of 2.4 Hz. Chemical shifts are reported relative to an external standard of 85% H_3PO_4. The sample was 1.5 mM $d(A^+\text{-}G)_{10}$ in residues in 1.4 mM Na^+/2.7 mM acetate/D_2O:H_2O (3:2), pH 4.05.

Molecular Modeling. Modeling was on an IBM PC, Intel 486DX, 66 MHz, 24 MB RAM with AMBER as part of HyperChem (Hyperchem 4.0, 1994). Parameters are those of AMBER 3.0A (Weiner et al., 1986), using the standard unmodified all-atom force field. Base charges for dA^+ are those for dA but with a proton on N_1 with a bond length of 1.1 Å (force constant of 14 kcal·mol^{-1}·Å^{-2}), bond angle of 117.4°, and torsion angle of 0.0° (force constants of 125 and 16 kcal·mol^{-1}·deg^{-2}, respectively) to maintain the proton in the plane of the purine ring. All calculations were done with a 0.5 fs time step (integration step) as the hydrogen atoms were not constrained. The initial conformation was generated by putting $d(A^+\text{-}G)_5$, a tractable length of oligomer, in the helical conformation of one of the strands of a B-DNA duplex and rotating every dA^+ residue ~180° to obtain an unstacked single strand.

In order to generate various conformations, a 22 ps, constant energy, constant volume (microcanonical ensemble), *high temperature molecular dynamics* simulation of $d(A^+\text{-}G)_5$ was performed. No cutoff distance was used for nonbonded interactions, and a distance-dependent dielectric constant, ϵ [ϵ = (permittivity of free space) × (scale factor) × (interatomic separation)], was used as a model solvent. For a highly charged system such as this, a dielectric constant scale factor of 4.0 was used (Weiner et al., 1984), and 1−4 scale factors were set at 0.5 for electrostatic and van der Waals interactions. Previous simulations using scale factors of 1 and 2 resulted in the dA^+ residues remaining in close proximity to the electronegative backbone oxygens, thereby restraining the conformational search. The starting temperature of the simulation was 0 K with temperature steps of 10 K taking the system to 3000 K in 0.15 ps; conformations (snapshots) were stored at 4000 time step intervals resulting in 11 conformations at 2 ps intervals.

To obtain a low-energy conformation, *simulated annealing* was done on the high temperature 2 ps conformation by cooling slowly from 3000 to 300 K in 0.5 K steps, with conformations stored every 0.25 ps. Conditions used were those of the high-temperature molecular dynamics.

Room temperature molecular dynamics was used to obtain the most favorable conformation. The structure obtained from the simulated annealing was placed in a periodic box, 26 × 26 × 56.1 Å [~1110 H_2O, TIP3P model (equilibrated at 300 K and 1 atm) (Jorgenson et al., 1983)]. At this stage, the 5′-dA residue was found to be noninteracting and set neutral; hence, five Na^+ ions were placed 1.7 Å equidistant from the oxygen atoms of the noninteracting phosphates and constrained to each oxygen with a force constant of 14 kcal·mol^{-1}·Å^{-2}. Using the AMBER protocol with explicit water molecules, the dielectric constant scale factor was set at 1.0, and 1−4 scale factors were set at 0.5 for electrostatic and van der Waals interactions. Nonbonding interactions were limited by a switched cutoff, with outer and inner radii of 13 and 9 Å, respectively. To allow for stable trajectories, this system was first energy minimized to an rms gradient of 10. A 10.625 ps constant temperature (300 K), constant volume (canonical ensemble) molecular dynamics simulation was performed to search for a low-energy conformation using a bath coupling constant of 0.1 ps and conformations stored every 0.125 ps.

The low-energy conformation obtained at the end of the room temperature simulation was *energy minimized* (with the same parameters) using a conjugate gradient method (Polak-Robiere) and convergence set at 0.1 kcal·Å^{-1}·mol^{-1} for the rms gradient. The resultant structure had a nonregular "bent" backbone conformation, ~13 Å in diameter and ~51 Å in length, formed by a lattice of unstacked dA^+ residues lying more or less parallel to the long axis, each translated ~12 Å and linked to its $n-1$ phosphate by both ionic and H-bond interactions, from which protrude noninteracting dG residues.

The above protocols (*simulated annealing, room temperature molecular dynamics, energy minimization*) were performed on the 4, 6, and 8 ps conformations obtained from the *high-temperature molecular dynamics* simulation. In these cases, the resultant structures showed the dA^+ residues interacting with the oxygens of the phosphodiester backbone, but with various nonregular backbone conformations.

Close inspection of the above structures showed that the dA^+—phosphate binding motif allows for conformational freedom between each "dinucleotide unit":

$$dA^+\text{—P-dG-P-}dA^+\text{—P-dG-P-}dA^+\text{—P-dG-P-}dA^+\text{—P-dG-P-}dA^+\text{—P-dG}$$

where the — bond indicates the site of conformational freedom (in particular, the α-torsion angle $O_{3'}$—P—$O_{5'}$—$C_{5'}$). We therefore chose the above 2 ps energy-minimized structure and changed the α-torsion angles (—) so as to obtain a more regular, nonbent backbone conformation. To remove any unfavorable interactions, a room temperature molecular dynamics simulation (canonical ensemble, with the same parameters) was performed and terminated after 3 ps with the potential energy (E_p) reaching a plateau at −20 572 kcal·mol^{-1}. The low-energy conformation obtained at the end of this simulation was energy minimized (with the same parameters, rms of 0.1 kcal·Å^{-1}·mol^{-1} etc. with a resultant E_p = −24 307 kcal·mol^{-1}) and is the model discussed in the text and shown in Figures 4 and 5 with Na^+ and H_2O removed.

RESULTS

S1 Nuclease Resistance. S1 nuclease has the ability to recognize perturbations of the phosphodiester backbone (Drew, 1984; Wells et al., 1988). Regular base-paired helices are resistant to this enzyme, whatever the helical form, whereas phosphodiester bonds adjacent to extrahelical residues and at B−Z junctions are readily cleaved, as are single-stranded polynucleotides, even when their bases are stacked in fluctuating helical arrays, e.g., poly(A) and poly(C) at neutrality.

To further characterize the helical structure of $d(A^+\text{-}G)_{10}$, studies of S1 nuclease sensitivity were carried out on it and

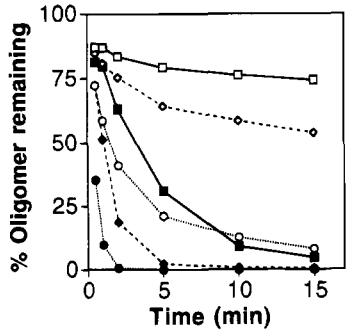

FIGURE 1: Kinetics of S1 nuclease digestion of $d(A^+-G)_{10}$ (open symbols) and $d(T)_{21}$ (solid symbols). The percent *full-length* oligomer remaining is shown at 5 (—), 20 (- - -), and 40 °C (•••).

a single strand devoid of secondary structure, $d(T)_{21}$, both at pH 4.0. $d(A)_{21}$ could not serve as a more appropriate control at pH 4.0 because short A-oligomers form acid duplexes (Applequist & Damle, 1965; Blake & Fresco, 1973). The fact that the kinetics of S1 cleavage of both $d(A)_{21}$ and $d(T)_{21}$ at pH 7.0 were found to be essentially the same (data not shown) justifies $d(T)_{21}$ as an appropriate control.

The results in Figure 1 demonstrate substantial resistance of the $d(A^+-G)_{10}$ helix relative to the sensitivity apparent for the unstacked single strand $d(T)_{21}$. Thus, at 5 °C, while the initial rate of product formed/min, i.e., anything shorter than full-length oligomer, is 19%, it is 23.6% at 20 °C and 48.6% at 40 °C. Moreover, 67% of full-length $d(A^+-G)_{10}$ remains after 60 min at 5 °C, 46% at 20 °C, and as much as 3% yet at 40 °C. It is also relevant that at 5 °C the helical structure of $d(A^+-G)_{10}$ (T_m 37 °C) is nearly 100% formed, while at 20 and 40 °C it is 87% and 42% intact, respectively (from thermal melting profiles), and that $d(A^+-G)_6$ has a T_m of 10−12 °C under identical conditions (Dolinnaya et al., 1993). In keeping with the much lower stability of $d(A^+-G)_6$, the cleavage pattern of $d(A^+-G)_{10}$ at lower temperatures (not shown) reveals that the main products are one to three residues long, suggesting that initial cleavage products, whatever their size, are rapidly digested preferentially over intact helices. However, at 40 °C the cleavage pattern of $d(A^+-G)_{10}$ appears more random, with many sites much more susceptible than at 5 and 20 °C, in keeping with the fact that the structure is 58% denatured and that melting of this helix is not very cooperative (Dolinnaya et al., 1993). By comparison, the initial rates of product formed/min for $d(T)_{21}$ for the same temperatures are 2−3 times those for $d(A^+-G)_{10}$, and digestion for only 2 min at 5 °C, or 1 min at 20 °C, leaves only 63% and 51% full-length oligomer, respectively. Moreover, the distribution of cleavage product sizes (not shown) appears random at all temperatures, in agreement with its complete lack of structure.

The presence of S1 hypersensitive sites has proved useful in identifying sequences involved in various non-B-DNA structures and in the characterization of their conformations (Wells et al., 1988; Rippe & Jovin, 1989). Interestingly, S1 nuclease hypersensitivity of $d(A-G)_n$•$d(C-T)_n$ sequences in plasmids and sometimes in linear DNA, together with chemical modification data, was used in the characterization of H-DNA. However, in assessing the sensitivity of a sequence to nuclease activity, it must be referred to another structure. In the case of H-DNA, the looped-out purine strand was shown to be hypersensitive compared to the adjacent duplex or triplex segments. Here we have used S1 nuclease to show that the helical structure, $d(A^+-G)_{10}$, is S1 nuclease resistant relative to the unstructured $d(T)_{21}$, which is randomly cleaved. This behavior is in keeping with the regular helical secondary structure proposed for $d(A^+-G)_{10}$.

UV Spectrum of dG Residues Selectively Perturbable. Shifts in the absorption spectrum of a chromophore are expected when it is exposed to a solvent whose refractive index is modified by some inert additive such as sucrose (Laskowski, 1966). However, spectral perturbation should not occur if the chromophore is prohibited from solvation [observed for nucleic acid duplexes and triplexes, but not for residues in loops, which are readily detectable by this method (J. A. Fossella, J. Berger, and J. R. Fresco, unpublished observations)]. This makes it possible to distinguish between chromophores accessible or inaccessible to solvent by virtue of their perturbation spectra. Perturbation by 50% sucrose was used to assess the relative exposure of the dG and dA residues of $d(A^+-G)_{10}$ to the solvent environment at 5 °C where the helix is stable and at 60 °C where it is fully denatured and the base residues are partially unstacked. This could be done because the CD spectrum at 5 °C is not significantly altered by 50% sucrose.

To evaluate the perturbation (*P*) spectra of the oligomer, reference *P* spectra of the monomers were determined in the same ionized states in which they occur in the helix at 5 °C and in the partially stacked single strand at 60 °C. Since it had been deduced that the dG residues are extrahelically situated in $d(A^+-G)_{10}$ (Dolinnaya & Fresco, 1992), the *P* spectrum of dGMP at pH 4.0 was taken as a reference standard for those residues in the oligomer at both 5 and 60 °C. The situation for the dA residues is more complicated. At pH 4.0, 5 °C, nine of the ten dA residues are fully protonated (Dolinnaya et al., 1993) and directly involved in the helical structure (see below); so, these residues might be constrained from solvation. As the remaining 5′-terminal dA residue has no upstream phosphate with which to form ionic and H-bonds, at pH 4.0, i.e., below the pK_a for dAMP, it should be ~60% protonated and fully solvated. In contrast, at pH 4.0, 60 °C, a substantial fraction of all the dA residues should be ~60% protonated and only partially solvated, because at that temperature they are partially stacked with their dG nearest neighbors. For these reasons, *P* spectra for dAMP were obtained at pH 3.0, 5 °C, and at pH 4.0, 60 °C, for reference standards at these temperatures.

Sucrose perturbation causes small, readily detectable red shifts that give rise to sharp positive and negative peaks in the *P* spectra, which are as singular for each base chromophore as the absorption spectra themselves. Thus, the *P* spectra for dGMP at 5 and 60 °C (Figure 2) show a negative peak at ~238 nm and positive peaks at 260 and 288 nm, while that for dAMP (Figure 2) shows a negative peak at 246 nm and a positive one at 272 nm at 5 °C that shifts to 274 nm at 60 °C.

To assess the solvation of the residues of $d(A^+-G)_{10}$, the UV spectra of the oligomer at pH 4.0 without and with 50% sucrose were recorded at 5 °C, where the helical secondary structure is fully developed, and at 60 °C, where that secondary structure is denatured, but the residues are partially stacked (Dolinnaya & Fresco, 1992). At 5 °C (Figure 2A) the *P* spectrum is very broad, rising from a minimum near 235 nm to a peak at 259 nm and slight shoulders near 270 and 288 nm. Although the dG monomer peak at 288 nm is

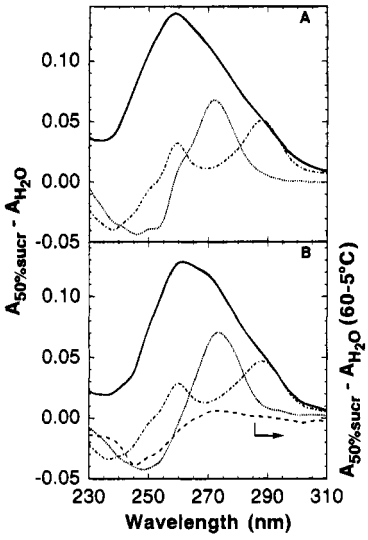

FIGURE 2: Comparison of UV perturbation (*P*) spectra of dAMP, dGMP, and $d(A^+\text{-}G)_{10}$ and of the change in the *P* spectrum on heating the helix. (A) 50% sucrose *P* spectra of $d(A^+\text{-}G)_{10}$ (—) and, for comparison, of dGMP (— • —) and dAMP (• • •) at 5 °C. (B) 50% sucrose *P* spectra of $d(A^+\text{-}G)_{10}$ (—) and, for comparison, *P* spectra of dGMP (— • —) and dAMP (• • •) at 60 °C; *P* difference spectrum (60−5 °C) of $d(A^+\text{-}G)_{10}$ and its partially melted single strand (- - -).

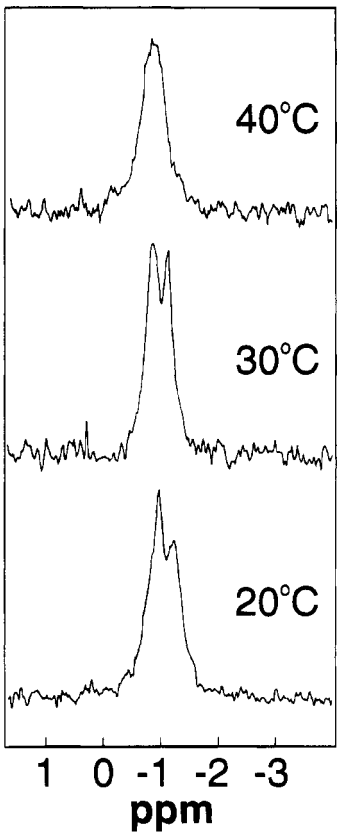

FIGURE 3: Proton-decoupled ^{31}P NMR spectra of $d(A^+\text{-}G)_{10}$ at 20, 30, and 40 °C.

substantially suppressed at 5 and 60 °C, the peak at 260 nm is prominent in the oligomer *P* spectra at both temperatures. This prominence suggests that the dG residues are solvated in both the helix and at 60 °C. In the *P* spectrum at 5 °C, it is also apparent from the major peak at 259 nm and only the barest indication of a shoulder near 272 nm that the contribution of the dA^+ residues is small, suggesting they are solvated to only a minor extent. It is apparent then that the dG residues of the helix are preferentially exposed to the solvent, consistent with their being extrahelically disposed.

At 60 °C the *P* spectrum (Figure 2B) contains indications of a double peak that has been broadened to the red, indicative of the superposition of the *P* spectrum for dA residues on that observed at 5 °C. This contribution is more easily discerned in the 60−5 °C *P difference* spectrum (Figure 2B). The character of that *difference* spectrum, which arises when the helix is thermally denatured, shows that it derives from the dA residues, viz. the broad shallow peak with λ_{min} and λ_{max} at 246 and 273 nm, respectively, coinciding with those for dAMP and an obvious absence of contributions of the λ_{min} at ~283 nm and λ_{max} at 260 nm from the *P* spectrum for dG. The peak at 273 nm in the 60−5 °C *P difference* spectrum would undoubtedly be larger, were it not for the partial stacking of the nearest neighbor dA and dG residues at 60 °C. Apparently, there is an increase in solvation of only the dA residues, which are no longer constrained by interaction with phosphates in the core of the helix.

These observations relate to the UV melting behavior of $d(A^+\text{-}G)_{10}$ (Dolinnaya & Fresco, 1992), which indicates very modest hypochromism for the helix but slight biphasic melting at 280 nm due to stacking of dG residues that were not stacked in the helix. Thus, the preferential perturbation of dG residues at low temperature, followed by preferential increase in perturbation of dA residues at high temperature, is consistent with partial inaccessibility to solvent of the dA residues at low temperature, whereas the dG residues are in substantial contact with the solvent. This is structurally reasonable since nine dA residues are an integral part of the helix, oriented such that only one of their surfaces may be partially accessible to the solvent (Figures 4 and 5) and the 5′-terminal dA residue is fully solvated.

Two Types of Phosphate Moieties. The secondary structure deduced for $d(A^+\text{-}G)_{10}$ predicts two types of backbone phosphates, nine bridged to positively charged dA residues by ionic and H-bonds and ten nonbonded. These two distinct phosphate environments ought to result in a well-resolved doublet ^{31}P NMR spectrum consisting of resonances of nearly comparable area.

Spectra were measured at 20, 30, and 40 °C, where the helix is 87%, 67%, and 42% formed (Dolinnaya et al, 1993). At 20 °C, there are, in fact, two ^{31}P resonances whose areas correspond to 55% and 40% at −1.0 and at −1.2 ppm, respectively, of the total ^{31}P resonance (Figure 3). Better resolution is obtained at 30 °C, where the downfield resonance moves from −1.0 to −0.9 while the upfield resonance remains at −1.2 ppm. At 40 °C, the upfield resonance downshifts and coalesces with the downfield resonance, resulting in a broad resonance centered about −0.85 ppm.

Data generated for DNA double helices show that internal phosphates exhibit upfield ^{31}P chemical shifts which move downfield upon thermal denaturation (Nikonowicz & Gorenstein, 1990; El Antri et al., 1993). While denaturation of $d(A^+\text{-}G)_{10}$ does not result in a comparable conformational change, it is reasonable to expect that its upfield ^{31}P resonance will also downshift at elevated temperatures. While it is not possible to assign the two ^{31}P chemical shifts,

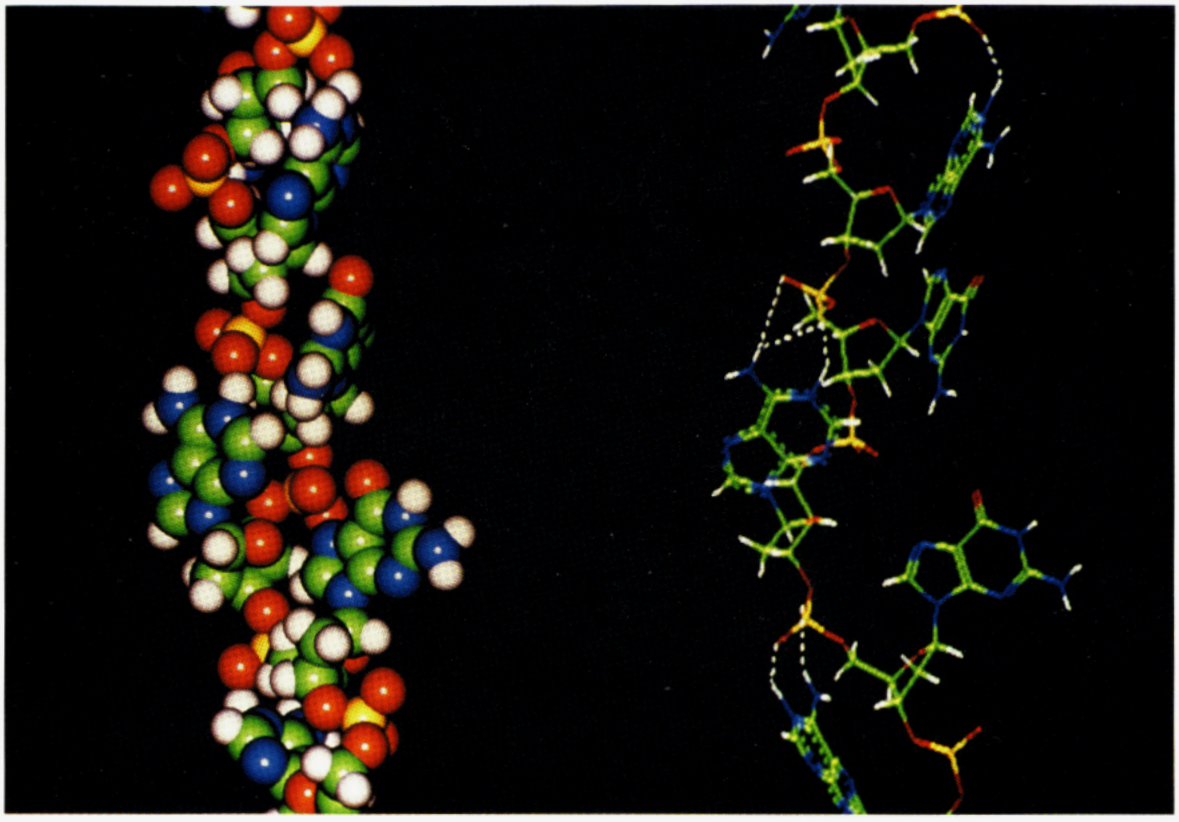

FIGURE 4: Five center residues of d(A^+-G)$_5$, i.e., 5′-d($pA^+_5pG_6pA^+_7pG_8pA^+_9$)-3′ showing ionic and H-bonds as indicated by white dashed lines (H_2O and Na^+ omitted for clarity). All structures are oriented 5′ → 3′ from top to bottom. (A) Left panel: space-filling representation. (B) Right panel: wire representation (similar perspective). Atom colors: C, green; N, blue; O, red; P, yellow; H, white.

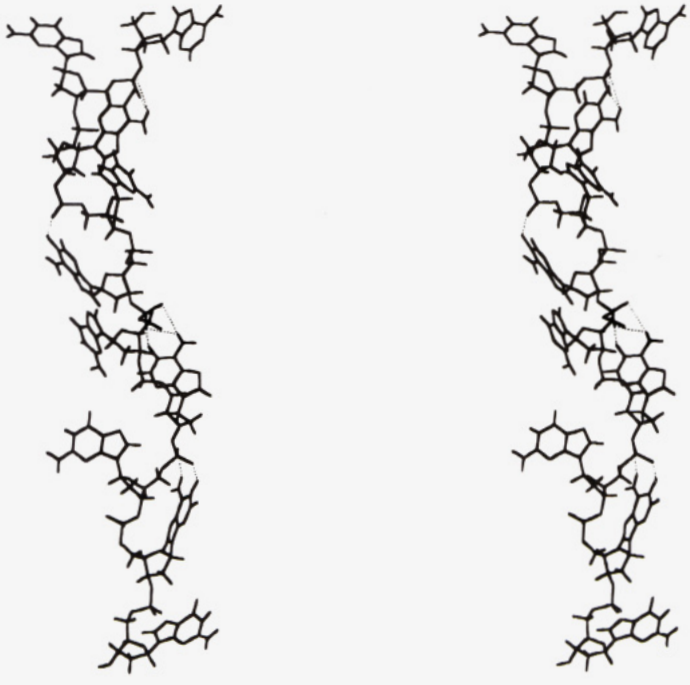

FIGURE 5: Stereoview of d(A^+-G)$_5$.

their occurrence provides evidence for two significantly different phosphodiester environments in the helix, one for the A^+pG segments with phosphates bridged by ionic and H-bonds to distal dA^+ residues and the other for the GpA^+ segments with noninteracting backbone phosphates.

dA^+−Phosphodiester Ionic and H-Bonds Stabilize the Secondary Structure. The model derived for d(A^+-G)$_5$ (Figures 4 and 5; see Experimental Procedures for details) reveals a helical structure ~12 Å in diameter and ~54 Å in length. It is formed by a lattice of unstacked dA^+ residues lying more or less parallel to the long axis, linked to the $n - 1$ phosphate oxygens, i.e., one phosphate upstream, by strong ionic and H-bonds mediated by $A-N_1H^+$ and $A-N_6H$, while the noninteracting dG residues protrude from the helix. The backbone conformation of this novel secondary structure is unlike any known duplex conformation

(Lavelle and Fresco, unpublished observations). However, the CD spectrum of $d(A^+\text{-}G)_{10}$ is remarkably like that of Z-DNA (Dolinnaya & Fresco, 1992), and the model does indicate a left-handed helical sense of backbone twist (Figure 5).

With the exception of dA_1, which is displaced due to the absence of an upstream phosphate with which to bond (Figure 5), the dA^+ residues are held very close and parallel, rather than perpendicular, to the backbone. The distance between the N_9 atoms of successive dA^+ residues is ~12 Å. While there is some variation in orientation about the glycosyl bonds, the torsion angle, χ, indicates an *anti* or high-*anti* conformation for all the residues. In this connection, it is important to note that the modeling was done with no constraints and that UV resonance Raman (UVRR) observations confirm that all the residues are in an *anti*-type conformation (Mukerji et al., 1995). There is no apparent interaction between the dG residues and any other component of the helix; rather, they are unrestricted and accessible to bulk solvent, just as indicated by the results of UVRR and solvent perturbation spectroscopies. In this regard, conformational heterogeneity is expected for the first (5′) dA residue (which lacks an upstream phosphate partner) and the dG residues, as they are relatively free to rotate about their glycosyl bond.

In sum, the calculations reveal a stable structure maintained by H-bond and Coulombic interactions between the dA^+ residues and the oxygens of the phosphodiester backbone. In the absence of the more typical base stacking and H-bonded base pairing, these must be the major interactions that stabilize the structure.

DISCUSSION

Structural Conclusions. The findings reported here and in the accompanying paper (Mukerji et al., 1995) confirm and elaborate on the structural characteristics deduced previously for the $d(A^+\text{-}G)_{10}$ helix (Dolinnaya & Fresco, 1992; Dolinnaya et al., 1993). (1) The S1 nuclease sensitivity assay reveals a structure with phosphodiester bonds comparatively insensitive to cleavage, as is characteristic of phosphodiester bonds in regular helical arrays, and may also be conferred by the base−backbone interactions. (2) The ^{31}P NMR spectra reveal two types of phosphate moieties, characterized by different chemical shifts, which move downfield as the structure is thermally denatured, until they coalesce to a single broad phosphate resonance at a temperature above T_m. The two types of phosphates would seem to correspond to those that are noninteracting and those forming ionic and H-bonds to the 9 dA^+ residues. (3) Sucrose perturbation spectroscopy shows the dG residues to be solvated, unlike the dA^+ residues which become so largely as a result of helix melting. (4) UVRR shows (Mukerji et al., 1995) a shift in the exocyclic amino scissors mode of dA^+ but not of dG residues. This not only confirms the intrahelical involvement of the dA^+ and extrahelical location of the dG residues but also provides direct evidence for H-bonds between $dA\text{−}N_6H_2$ and the electronegative oxygens of the phosphates. Also, a shift is seen in vibrational modes consistent with the protonation of N_1 of dA residues. (5) The molecular modeling gives a clearer definition of the secondary structure first glimpsed indirectly from solution studies. It is particularly impressive that the energy-minimized structure contains the full variety of noncovalent interactions, base dispositions, and left-handed helical sense, independently demonstrated by the various spectroscopic observations.

In evaluating the significance of these findings, it is important to recognize their consistency with the earlier proposed secondary structural model and earlier titrimetric, calorimetric, UV absorption, and CD spectroscopic observations (Dolinnaya & Fresco, 1992; Dolinnaya et al., 1993). Such cumulative confirmation is highly unlikely to stem from coincidence. We note also that we have been unable to derive an alternative secondary structural model to fit the totality of the observations.

Similarity to the Protein α-Helix. In comparing $d(A^+\text{-}G)_{10}$ to other biopolymers, one is struck by its similarity in both structural organization and physical properties to α-helical polypeptides. For hydrophilic polypeptides such as polylysine and polyglutamic acid, the optical changes accompanying their pH and thermally induced helix → coil transitions are not unlike those observed for the comparable transition for $d(A^+\text{-}G)_{10}$ (Dolinnaya et al., 1993) which, different from other types of nucleic acid helices, exhibits no evidence of base stacking or base pairing (Dolinnaya & Fresco, 1992). Rather, $d(A^+\text{-}G)_{10}$ is a single-stranded helical oligomer whose dA^+ side-chain residues and backbone provide a helical core with stabilizing interactions approximately parallel to the helix axis and whose dG constituents protrude into the surrounding solvent. The analogy with the properties of the protein α-helix is also indicated by the moderate cooperativity in proton uptake, partially melted intermediate states, and rise in apparent pK_a with oligomer length shown by $d(A^+\text{-}G)_{10}$ (Dolinnaya et al., 1993).

Structural and Biological Implications. We have previously suggested possible biological roles for the single-stranded helix of $d(A^+\text{-}G)_{10}$ (Dolinnaya & Fresco, 1992; Dolinnaya et al., 1993) and that protein binding could stabilize the structure under physiological conditions. The new type of secondary structure described here need not be restricted to the alternating d(A-G) sequence nor to the deoxyribo backbone, so there are likely to be sequence-specific variants, i.e., a family of such structures, just as there are α, π, and 3_{10} polypeptide helices. In fact, the modeling indicates that the interactions stabilizing the helical structure are capable of greater sequence versatility than has been tested with the simple alternating A-G sequence (Lavelle and Fresco, unpublished observations). In this respect, C and T residues possess the chemical features to serve analogously to the A and G residues of $d(A^+\text{-}G)_{10}$, i.e., to form ionic bonds with backbone phosphates [essentially at neutrality (Lavelle & Fresco, 1995)] and to serve as "spacers", respectively. Thus, we can imagine other sequences, particularly repetitive ones, with even all four bases, for which some type of single-stranded helical array stabilized by longitudinal rather than horizontal interactions relative to the helix axis represents the optimal energy minimum. Such sequences abound in eukaryotic genomes, and their extension has in some cases been associated with a number of genetic diseases [Verkerk et al., 1991; also see reviews by Miwa (1994) and Sutherland and Richards (1994)]. So it would not surprise us if they are found to exhibit a variety of structural and functional consequences in biological systems. This type of single-stranded *secondary structure* also provides a possible basis for a replicative mechanism that may generate aberrant genomic repetitive sequences, and it could

have served a stabilizing role for the accumulation and evolution of primordial nucleic acid sequences.

ACKNOWLEDGMENT

We are grateful to Jannette Carey for suggesting the possibility of heterogeneity in the ^{31}P chemical shift spectrum and to Robert Pascal, Jr., for help with the NMR measurements.

REFERENCES

Applequist, J., & Damle, V. N. (1965) *J. Am. Chem. Soc. 87*, 1450−1458.

Blake, R. D., & Fresco, J. R. (1973) *Biopolymers 12*, 775−789.

Dolinnaya, N. G., & Fresco, J. R. (1992) *Proc. Natl. Acad. Sci. U.S.A. 89*, 9242−9246.

Dolinnaya, N. G., Braswell, E. H., Fossella, J. A., Klump, H., & Fresco, J. R. (1993) *Biochemistry 32*, 10263−10270.

Drew, H. R. (1984) *J. Mol. Biol. 176*, 535−557.

El Antri, S., Mauffret, O., Monnot, M., Lescot, E., Convert, O., & Fermandjian, S. (1993) *J. Mol. Biol. 230*, 373−378.

Fossella, J. A., Kim, Y. J., Shih, H., Richards, E. G., & Fresco, J. R. (1993) *Nucleic Acids Res. 21*, 4511−4515.

Fresco, J. R., & Doty, P. (1957) *J. Am. Chem. Soc. 79*, 3928−3929.

HyperChem 4.0 (1994) Hypercube Corporation, Waterloo, Ontario, Canada.

Jorgensen, W. L., Chandrasekhar, J., Madura, J. D., Impey, R. W., & Klein, M. L. (1983) *J. Chem. Phys. 79*, 926−935.

Laskowski, M., Jr. (1966) *Fed. Proc. 25*, 20−27.

Lavelle, L., & Fresco, J. R. (1995) *Nucleic Acids Res. 23*, 2692−2705.

Miwa, S. (1994) *Nature Genet. 6*, 3−4.

Mukerji, I., Shiber, M. C., Spiro, T. G., & Fresco, J. R. (1995) *Biochemistry 34*, 14300−14303.

Nikonowicz, E. P., & Gorenstein, D. G. (1990) *Biochemistry 29*, 8845−8858.

Rippe, K., & Jovin, T. M. (1989) *Biochemistry 28*, 9542−9549.

Sutherland, G. R., & Richards, R. I. (1994) *Am. Sci. 82*, 157−163.

Verkerk, A. J. M. H., et al. (1991) *Cell 65*, 905−914.

Weiner, S. J., Kollman, P. A., Case, D. A., Singh, U. C. Ghio, C., Alagona, G., Profeta, S., Jr., & Weiner, P. (1984) *J. Am. Chem. Soc. 106*, 765−784.

Weiner, S. J., Kollman, P. A., Nguyen, D. T., & Case, D. A. (1986) *J. Comput. Chem. 7*, 230−252.

Wells, R. D., Collier, D. A., Hanvey, J. C., Shimizu, M., & Wohlrab, F. (1988) *FASEB J. 2*, 2939−2949.

BI942902G